Supporting Information Appendix S1

Crystal structures indicate distinctly altered and charged binding pockets

To gain molecular insights into their activity, substrate specificity (see below) and classification, we first attempted to crystallise each of the deep-sea α/β-hydrolases. MGS-M1, MGS-M2 and MGS-MT1 were successfully crystallised, and their structures were solved by molecular replacement using their closest PDB homologues (Supporting Information Figs. S3–S4). Analysis of these crystal structures revealed key active site characteristics that were distinct relative to other structurally characterised α/β hydrolases (i.e., sequence substitutions).

The only two significant structural homologues of MGS-M1 were the putative carboxylesterase Cest-2923 (PDB code 4BZW, Z-score 14.7, Benavente *et al.*, 2013; Supporting Information Fig. S3) and the BES protein from *Bacillus anthracis* (PDB 2QM0, Z-score 8.7). Both of these enzymes and MGS-M1 were categorised by the 3DM database (Kourist *et al.*, 2010) as "unclassified" α/β-hydrolases. The overall electrostatic charge on the surface of MGS-M1 resembled those of Cest-2923 and BES (Fig. 5), with no obvious patches of concentrated charge. MGS-M1 also shared with these enzymes the absence of a significant cap subdomain modulating the size and accessibility of the substrate-binding cavity. However, MGS-M1 contained a deletion of 14 amino acids relative to Cest-2923 in this region (residues 141–150 in MGS-M1 and 158–181 in Cest-2923), which resulted in alterations in the shape and accessibility of the active site. The active site cleft of MGS-M1 was significantly larger than that of Cest-2923; in fact, the crystal structure of MGS-M1 contained electron density bound in this region of the active site that we modelled as a polyethylene molecule (Supporting Information Fig. S4), which could mimic a substrate; this region in Cest-2923 was inaccessible. Residue-by-residue analysis of the active sites of these two enzymes showed the conformation of residues essential for catalysis, as well as the amino acids nearest to these core elements; however, important distinctions were observed in the residues lining the substrate-binding canal. In total, 11 of 16 residues in the MGS-M1 substrate-binding cavity were conserved in Cest-2923 (Supporting Information Fig. S4); the 5 non-conserved residues were found in the divergent cap region known to play a role in substrate specificity (Kourist *et al.*, 2010). These structural properties and the larger active site of MGS-M1 compared to Cest-2923 were consistent with the difference in preferences acyl chain length of *p*NP esters between these enzymes: Cest-2923 exhibited less than 20% activity against lengths of C8 and longer (Benavente *et al.*, 2013), while MGS-M1 retained approximately 60% activity against a substrate of length C12 (Supporting Information Fig. S2). Interestingly, other characteristics of MGS-M1 and Cest-2923 are similar, including temperature profile (both enzymes have optimal activity at approximately 30 ºC), optimal pH (8.0 and 7.0, respectively) and

calculated *p*I (5.8 vs. 6.3, respectively). Overall, this analysis reveals that MGS-M1 contains unique active site architecture.

The crystal structure of MGS-M2 was consistent with its categorisation into esterase/lipase alpha/beta family V, which also includes *meta*-cleavage product (MCP) hydrolases. The closest structural homologues identified by the PDBeFold server of MGS-M2 included the MCP hydrolases CumD from *Pseudomonas fluorescens* IP01 (PDB 1IUN, Fushinobu *et al.*, 2002), HsaD from *Mycobacterium tuberculosis* (PDB 2WUG, Lack *et al.*, 2010) and the enol-lactonase from *Burkholderia xenovorans* LB400 (PDB 2XUA, Bains *et al.*, 2011), with Z-scores of approximately 14 and RMSD values of 1.8–2.0 over nearly the full length of MGS-M2 (approximately 250 of 276 residues), indicating significant structural similarity. MGS-M2 shares the core α/β-hydrolase fold of these enzymes, along with a large cap subdomain (residues 125–195) that covers the catalytic centre and shapes the substrate-binding cavity (Supporting Information Figs. S3–S4). The similarity in structure between MGS-M2 and the MCP hydrolases could be extended to the shape of the active site, and the ligand 2-hydroxy-6-oxo-6-phenylhexa-2,4-dienoic acid (HOPDA) bound to HsaD is accommodated in the MGS-M2 active site upon superposition of the respective enzyme structures (Supporting Information Fig. S4). However, MGS-M2 has different electrostatic characteristics and residue composition: the active sites of the MCP hydrolases are noticeably positively charged, while that of MGS-M2 contains a mixture of positive and negative features (Fig. 6). As an example of a key residue substitution involved in this charge difference, the residue Leu117 in MGS-M2 is replaced in MCP hydrolases by an arginine (HsaD Arg192), which interacts with the carboxylate of HOPDA. While the similarity in overall structure confidently categorises MGS-M2 into family V with MCP hydrolases, the distinct features of its active site imply that MGS-M2 is not an MCP hydrolase, as was further confirmed by assays (Alcaide *et al.*, 2013). Finally, the size of the active site of MGS-M2 is consistent with the experimentally determined substrate range in this study, as *p*NP esters as large as dodecanoate can be accommodated (Supporting Information Fig. S2).

The structure of MGS-MT1 is consistent with its classification in family IV (hormone-sensitive lipase, HSL) because its closest structural homologues in the PDB database are HSLs from thermophilic archaea, including AFEST from *Archaeoglobus fulgidus* (PDB 1JJI; De Simone *et al.*, 2001), EST2 from *Alicyclobacillus acidocaldarius* (PDB code 1EVQ; De Simone *et al.*, 2000) and ESTE1 from a metagenomic library (PDB 2C7B; Byun *et al.*, 2007) (Z-scores of approximately 12 and RMSD values between 1.6 and 1.75 Å over approximately 275 of the 315 Cα atoms of the MGS-MT1 crystal structure). Overall, the structure of MGS-MT1 is well conserved with these HSL enzymes, including the involvement of the N-terminus (residues 31–65) and an internal

insertion (residues 226–270) forming an all α-helical cap subdomain covering the catalytic centre (Supporting Information Fig. S3). The MGS-MT1 active site is long, deep, negatively charged and open to solvent (Fig. 6); this electrostatic characteristic is in sharp contrast to the properties of the HSL enzymes listed above, which vary in their size, charge and accessibility to solvent. Furthermore, the active site composition of MGS-MT1 is distinct from that of its HSL structural homologues (Supporting Information Fig. S4). The size and charge of the active site are consistent with the ability of MGS-MT1 to hydrolyse the larger compounds tri-O-acetyl-glucal and α-D-glucose pentaacetate (Supporting Information Fig. S2). Overall, these comparisons suggest that while MGS-MT1 can be categorised as a family IV α/β-hydrolase, as we observed for the other MGS esterase crystal structures, nevertheless, MGS-MT1 contains specific amino acid substitutions in the active site, i.e., the aligned residues MGS-MT1 Trp224, Leu251 and Phe292 *vs.* AFEST Val190, Met215 and Leu257 (Supporting Information Fig. S4), which predict a different substrate specificity from that of its structural homologues.

We also crystallised and determined the structures of the aldo-keto reductase MGS-M4 and the (*L*)-lactate dehydrogenase MGS-M5. The structure of MGS-M4 has a TIM-barrel fold (Dellus-Gur *et al.*, 2013) and was very well conserved with the structures of more than 50 NADPH-dependent aldo-keto reductases from the Pfam family PF00248 (Z-scores between 17–21 and RMSD values between 0.8 and 1.2 Å over the full 274 residue MGS-M4 sequence) (Supporting Information Fig. S3). The binding of NADPH by PF00024 family enzymes involves atoms from 12 residues in a positively charged pocket; in MGS-M4, 11 of these 12 residues are conserved, and a positively charged pocket is present, suggesting that the binding of NADPH to this enzyme would be largely similar to that in its structural homologues. Aldo-keto reductases have substrate binding sites with diverse size, depth and charge, based on which different substrates can be accommodated. MGS-M4 contains a small (153 Å^3), slightly positively charged binding site. One of the top structural homologues is prostaglandin F synthase, which contains a large, extended and positively charged substrate binding site. A comparison of the prostaglandin F synthase and MGS-M4 active sites showed some similarities and some differences (Supporting Information Fig. S4): the MGS-M4 active site is smaller and is missing some structural loops involved in substrate contacts, but there are numerous identical or similar residues in the active site; these residues are likely involved in catalysis and/or for reducing contacts with the core ketone moiety.

The structure of MGS-M5 matched conclusively to more than 100 L-lactate dehydrogenase enzymes from various bacteria (Z-scores ranging from 16.0 to 18.6 and RMSD values between 0.8 and 1.3 Å over approximately 300 residues of the MGS-M5 sequence) (Supporting Information

Fig. S3). A comparison of the electrostatic surface and active site composition of MGS-M5 revealed that it closely resembled the structures of other L-lactate dehydrogenase enzymes (Supporting Information Fig. S4), including the four residues involved in interacting with the pyruvate/L-lactate ligands.

Substrate fingerprint of deep-sea enzymes

A total of 158 chemicals were used to evaluate substrate ranges and specific activities (units/mg) (Supporting Information Fig. S2): (i) esterase-like substrates including 15 model esters (6 *p*-nitrophenols [*p*NPs], 3 α-naphthyls and 6 triacylglycerols) and a battery of 86 structurally different esters (for details, see Martínez-Martínez *et al.*, 2013); (ii) glycosidase-like substrates including 15 model sugars (including *p*NP derivatives and cellulooligosaccharides); (iii) aldo-keto reductase-like substrates including 41 model aldehydes and ketones; and (iv) the dehydrogenase-like substrates including sodium pyruvate. Substrate fingerprints (Supporting Information Fig. S2) revealed that MGS-M3 (11), MGS-M1 (12), MGS-M2 (13), and MGS-MT1 (16) showed the most restricted substrate profiles, whereas MGS-K1 (21), MGS-B1 (26), MGS-HA1 (33), and MGS-M4 (41) showed the widest substrate profiles; the numbers in parentheses indicate the numbers of substrates utilised by the enzymes.

All ester-hydrolases from the α/β-hydrolase family preferred short-to-medium size *p*NP-esters, triacylglycerols and alkyl and aryl esters, albeit to different extents (Supporting Information Fig. S2), supporting their predicted esterase function. The ability to hydrolyse halogenated (including those containing bromo, chloro, fluoro and iodo) alkyl and aryl esters was tested and only demonstrated for MGS-M2 (1 ester), MGS-B1 (5 esters), MGS-K1 (3 esters), and MGS-HA1 (9 esters). In contrast, MGS-M2, MGS-K1, and MGS-HA1 were only able to degrade bromide-containing esters. This result suggests that the high Br^- concentration in DHAB-like environments (Daffonchio *et al.*, 2006; Yakimov *et al.*, 2007a, 2007b; La Cono *et al.*, 2011; Yakimov *et al.*, 2011; Smedile *et al.*, 2012; Ferrer *et al.*, 2012; Yakimov *et al.*, 2013) may have selected for bromide-acting enzymes. All enzymes (as exemplified by MGS-M2, MGS-MT1, MGS-B1, MGS-K1, and MGS-HA1) are able to accept tri-O-acetyl-glucal and the carbohydrate ester α-D-glucose pentaacetate. In addition, hydroxycinnamic-like esters, such as methyl ferulate (for MGS-HA1) and methyl sinapinate (for MGS-K1), were also accepted as substrates by three enzymes. These results suggest that at least six of the deep-sea enzymes described herein can support polysaccharide degradation, which is critical for ecological success in deep-sea environments (Werner *et al.*, 2014). Finally, under our assay conditions, all esterases were also enantio-selective for 5 chiral esters (Supporting Information Fig. S2). Based on at least 2-fold relative specific

activities for separate enantiomers, a tentative indication of the best substrate preference and apparent enantiomeric ratio was found for MGS-K1 (> 300 for (*S*)-methyl-3-bromo-2-methyl propionate).

As shown in Supporting Information Fig. S2, the purified family 3 glycosidase protein MGS-M3 hydrolysed 6 of the 15 *p*NP derivatives tested, with *p*NP-β-D-glucopyranoside being the preferred substrate and *p*NP-β-D-galactopyranoside the less preferred substrate (~16-fold difference). Derivatives of β-lactose, β-xylose, β-cellobiose and α-arabinofuranose were also good substrates for the enzyme. The enzyme hydrolysed all short cello-oligosaccharides tested (degree of polymerisation [DP] from 2 to 5), with cellobiose being preferred. Based on its substrate profile, this family 3 glycosidase (http://www.cazy.org; Cantarel *et al.*, 2009) may be considered to be a β-glucosidase.

The purified recombinant protein MGS-M4, a putative (as indicated by a BLASTP search) aldo-keto reductase, exhibited activity towards 41 aldehydes and ketones (Supporting Information Fig. S2). Methyl-glyoxal was the best substrate, while reduced activity was observed when ethyl-3-oxohexanoate was used as the substrate. The enzyme efficiently reduced aromatic derivatives such as 4-nitrobenzaldehyde, benzaldehyde, phenylacetaldehyde, phenylglycol, 3-pyridinecarboxaldehyde, 4-pyridinecarboxaldehyde and isatin; it was also active towards alkyl and alkenyl (i.e., acrolein, 2-hexenal and ethyl-2-allylacetoacetate) substrates.

Finally, the purified recombinant protein MGS-M5, a putative (by meaning of BLASTP search) L-lactate dehydrogenase, was characterised, and its dehydrogenase activity was confirmed using sodium pyruvate as a substrate (Supporting Information Fig. S2).

These results suggest that the enzymes examined, which encompassed all deep-sea regions, can support polysaccharide component degradation, which occurs in algae and seagrass. This activity plays a role in ecological success in deep-sea environments (Werner *et al.*, 2014), as many classes of polysaccharides within the algal lineages appear to be highly diverse in terms of their sugar content and conformation, degree of sulphation, esterification, molecular weight and the presence of volatile compounds, including ketones and aldehydes (Guschina *et al.*, 2006; Kamenarska *et al.*, 2002). Therefore, the complete assimilation of algal components by deep-sea microbes may require appropriate enzyme cocktails, with three major enzymes needed: ester- and sugar-hydrolases and aldo-keto reductases. Therefore, the present study suggests that polysaccharide components may be major substrates for enzymes in deep-sea regions.

Supporting references

Bains, J., Kaufman, L., Farnell, B., and Boulanger, M.J. (2011). A product analog bound form of 3-

oxoadipate-enol-lactonase (PcaD) reveals a multifunctional role for the divergent cap domain. *J Mol Biol* **406:** 649-658.

Benavente, R., Esteban-Torres, M., Acebron, I., De Las Rivas, B., Muñoz, R., Alvarez, Y., and Mancheño, J.M. (2013). Structure, biochemical characterization and analysis of the pleomorphism of carboxylesterase Cest-2923 from *Lactobacillus plantarum* WCFS1. *FEBS J* **280:** 6658-6671.

Byun, J.S., Rhee, J.K., Kim, N.D., Yoon, J., Kim, D.U., Koh, E., *et al.* (2007). Crystal structure of hyperthermophilic esterase EstE1 and the relationship between its dimerization and thermostability properties. *BMC Struct Biol* **7:** 47.

Corbari, L., Zbinden, M., Cambon-Bonavita, M-A., Gail, F., and Compère, P. (2008). Bacterial symbionts and mineral deposits in the branchial chanber of the hydrothermal vent shrimp *Rimicaris exoculata*: relationship to moult cyle. *Aquatic Biol* **1:** 225-238.

De Simone, G., Galdiero, S., Manco, G., Lang, D., Rossi, M., and Pedone, C. (2000). A snapshot of a transition state analogue of a novel thermophilic esterase belonging to the subfamily of mammalian hormone-sensitive lipase. *J Mol Biol* **303:** 761-771.

De Simone, G., Menchise, V., Manco, G., Mandrich, L., Sorrentino, N., Lang. D., *et al.* (2001). The crystal structure of a hyper-thermophilic carboxylesterase from the archaeon *Archaeoglobus fulgidus*. *J Mol Biol* **314:** 507-518.

Dellus-Gur, E., Toth-Petroczy, A., Elias, M., and Tawfik, D.S. (2013). What makes a protein fold amenable to functional innovation? Fold polarity and stability trade-offs. *J Mol Biol* **425:** 2609-2621.

Fushinobu, S., Saku, T., Hidaka, M., Jun, S.Y., Nojiri, H., Yamane, H., *et al.* (2002). Crystal structures of a meta-cleavage product hydrolase from *Pseudomonas fluorescens* IP01 (CumD) complexed with cleavage products. *Protein Sci* **11:** 2184-2195.

Guschina, I.A., and Harwood, J.L. (2006). Lipids and lipid metabolism in eukaryotic algae. *Prog Lipid Res* **45:** 160-186.

Jean-Luc, C., Jean-Pierre, D., Yves, F., Jean-Baptiste, P., and Holm, N. (2002). Geochemistry of high H_2 and CH_4 vent fluids issuing from ultramafic rocks at the Rainbow hydrothermal field (36 degress 14'N, MAR). *Chem Geol* **191:** 345-359.

Kamenarska, Z., Dimitrova-Konaklieva, S., Stefanov, K., Najdenski, H., and Popov, S. (2002). Comparative study of the volatile compounds from some Black Sea brown algae. *Bot Mar* **45:** 502-509.

Lack, N.A., Yam, K.C., Lowe, E.D., Horsman, G.P., Owen, R.L., Sim, E., and Eltis, L.D. (2010). Characterization of a carbon-carbon hydrolase from *Mycobacterium tuberculosis* involved in

cholesterol metabolism. *J Biol Chem* **285:** 434-443.

Lai, K.K., Stogios, P.J., Vu, C., Xu, X., Cui, H., Molloy, S., *et al.* (2011). An inserted α/β subdomain shapes the catalytic pocket of *Lactobacillus johnsonii* cinnamoyl esterase. *PLoS One* **6:** e23269

Supporting Tables

Table S1 General features of reported enzymes isolated from deep-sea regions. The data are based on bibliographic records that are specifically cited.

Source	Enzyme description	Substrates tested, kinetic parameters and pH and temperature optima[1]	Reference
Deep-sea cultivable microorganism			
Extremely thermophilic methanogen *Methanococcus jannaschii* isolated from deep-sea hidrotermal vent	1 Protease	Opt. pH: 7.5-7.8 Opt Temp.: 116-130ºC Salt dependence: not reported	Michels PC, Clark DS. (1997). Pressure-enhanced activity and stability of a hyperthermophilic protease from a deep-sea methanogen. Appl Environ Microbiol 63:3985-3991
Deep-sea *Microbulbifer* JAMB-A7 isolated from Sagami Bay, Japan, at a depth of 1,174 m	1 β-Agarase	Opt. pH: 5.0-8.0 Opt Temp.: 46ºC Salt dependence: not reported	Ohta Y, Hatada Y, Nogi Y, Miyazaki M, Li Z, Akita M, *et al.* (2004). Enzymatic properties and nucleotide and amino acid sequences of a thermostable beta-agarase from a novel species of deep-sea *Microbulbifer*. Appl Microbiol Biotechnol 64:505-514
Hyperthermophilic *Thermococcus* strain HJ21 from a deep-sea hydrothermal vent	1 α-Amylase	Opt. pH: 5.0 Opt Temp.: 95ºC Salt dependence: 2.0 M NaCl optimal concentration	Wang S, Lu Z, Lu M, Qin S, Liu H, Deng X, *et al.* (2008). Identification of archaeon-producing hyperthermophilic alpha-amylase and characterization of the alpha-amylase. Appl Microbiol Biotechnol 80:605-614.
Deep-Sea chemolithoautotroph *Thiomicrospira crunogena*	4 Carbonic anhydrases	Opt. pH: not reported Opt Temp.: not reported Salt dependence: not reported	Dobrinski KP, Boller AJ, Scott KM. (2010). Expression and function of four carbonic anhydrase homologs in the deep-sea chemolithoautotroph *Thiomicrospira crunogena*. Appl Environ Microbiol 76:3561-3567.
Deep-sea clam *Calyptogena kaikoi*	1 two-domain arginine kinase	Opt. pH: not reported Opt Temp.: not reported Salt dependence: not reported	Uda K, Yamamoto K, Iwasaki N, Iwai M, Fujikura K, Ellington WR, Suzuki T. (2008). Two-domain arginine kinase from the deep-sea clam *Calyptogena kaikoi*-evidence of two active domains. Comp Biochem Physiol B Biochem Mol Biol 151:176-182.
Deep-Sea *Thermococcus siculi* strain HJ21 rom a deep-sea hydrothermal vent	1 Glycosyl hydrolase from the family 57 (GH57) or amylopullulanase	Opt. pH: 5.0-6.0 Opt Temp.: 95ºC Salt dependence: not reported	Jiao YL, Wang SJ, Lv MS, Xu JL, Fang YW, Liu S. (2011). A GH57 family amylopullulanase from deep-sea *Thermococcus siculi*: expression of the gene and characterization of the recombinant enzyme. Curr Microbiol 62:222-228.
Psychropiezophile *Moritella profunda*	1 Dihydrofolate reductase	Opt. pH: 7.0 Opt Temp.: 38ºC Salt dependence: not reported	Evans RM, Behiry EM, Tey LH, Guo J, Loveridge EJ, Allemann RK. (2010). Catalysis by dihydrofolate reductase from the psychropiezophile *Moritella profunda*. Chembiochem 11:2010-2017.
Deep-sea psychrophilic bacterium strain DY-A	1 Protease	Opt. pH: 10.0 Opt Temp.: 40ºC Salt dependence: not reported	Zeng R, Zhang R, Zhao J, Lin N. (2003). Cold-active serine alkaline protease from the psychrophilic bacterium *Pseudomonas* strain DY-A: enzyme purification and characterization. Extremophiles 7:335-337.
Deep-sea psychrotrophic bacterium *Pseudoalteromonas* sp. DY3	1 Cellulase	Opt. pH: 6.0-7.0 Opt Temp.: 40ºC Salt dependence: not reported	Zeng R, Xiong P, Wen J.(2006). Characterization and gene cloning of a cold-active cellulase from a deep-sea psychrotrophic bacterium *Pseudoalteromonas* sp. DY3. Extremophiles 10:79-82.
Deep-sea bacterium *Agarivorans* sp.	1 Alginate lyase	Opt. pH: 8.0-9.0 Opt Temp.: 40ºC Salt dependence: 0.2-0.8 M NaCl optimal concentration	Kobayashi T, Uchimura K, Miyazaki M, Nogi Y, Horikoshi K. (2009). A new high-alkaline alginate lyase from a deep-sea bacterium *Agarivorans* sp. Extremophiles 13:121-129.

Deep-sea psychrotolerant bacterium *Pseudoalteromonas* sp. SM9913	1 Subtilase	Opt. pH: 8.0 Opt Temp.: 15ºC Salt dependence: 3 M NaCl/KCl optimal concentration	Yan BQ, Chen XL, Hou XY, He H, Zhou BC, Zhang YZ. (2009). Molecular analysis of the gene encoding a cold-adapted halophilic subtilase from deep-sea psychrotolerant bacterium *Pseudoalteromonas* sp. SM9913: cloning, expression, characterization and function analysis of the C-terminal PPC domains. Extremophiles 13:725-733.
Psychrophilic deep-sea bacterium *Pseudomonas* sp. MM15	1 GH5 endoglucanase	Opt. pH: 4.5 Opt Temp.: 30ºC Salt dependence: not reported	Yang J, Dang H. (2011). Cloning and characterization of a novel cold-active endoglucanase establishing a new subfamily of glycosyl hydrolase family 5 from a psychrophilic deep-sea bacterium. FEMS Microbiol Lett 325:71-76.
Methanarchaeon *Methanocaldococcus jannaschii* from a deep-sea hydrothermal vent	1 Coenzyme F420-dependent sulfite reductase	Opt. pH: not reported Opt Temp.: not reported Salt dependence: not reported	Johnson EF, Mukhopadhyay B. (2005). A new type of sulfite reductase, a novel coenzyme F420-dependent enzyme, from the methanarchaeon *Methanocaldococcus jannaschii*. J Biol Chem 280:38776-38786.
Antarctic deep-sea psychrotrophic Bacterium, *Psychrobacter* sp. 7195	1 Lipase	Opt. pH: 9.0 Opt Temp.: 30ºC Salt dependence: no activations by cations	Zhang J, Lin S, Zeng R. (2007). Cloning, expression, and characterization of a cold-adapted lipase gene from an antarctic deep-sea psychrotrophic bacterium, *Psychrobacter* sp 7195. J Microbiol Biotechnol 17:604-610.
Deep-sea *Kocuria* sp. Mn22	1 Cellulase	Opt. pH: 8.5 Opt Temp.: 55ºC Salt dependence: no activations by cations	Chanjuan L, Hong Y, Shao Z, Lin L, Huang X, Liu P, Wu G, Meng X, Liu Z. (2009). Novel alkali-stable, cellulase-free xylanase from deep-sea *Kocuria* sp. Mn22. J Microbiol Biotechnol 19:873-880.
Deep-sea *Demequina* sp. JK4	1 Bifunctional xylanase	Opt. pH: 5.5 Opt Temp.: 55ºC Salt dependence: no activations by cations	Meng X, Shao Z, Hong Y, Lin L, Li C, Liu Z. (2009). A novel pH-stable, bifunctional xylanase isolated from a deep-sea microorganism, *Demequina* sp. JK4. J Microbiol Biotechnol 19:1077-1084.
Aerobic hyperthermophilic archaeon *Aeropyrum camini* from a deep-sea hydrothermal vent chimney	1 Oxygen-thermostable hydrogenase	Opt. pH: 8.5-9.0 Opt Temp.: 85ºC Salt dependence: not reported	Nishimura H, Sako Y. (2009). Purification and characterization of the oxygen-thermostable hydrogenase from the aerobic hyperthermophilic archaeon *Aeropyrum camini*. J Biosci Bioeng 108:299-303.
Deep-sea *Vibrio* sp. JAM-A9m	3 Alginate lyases	Opt. pH: 7.6-9.0 Opt Temp.: 30ºC Salt dependence: In the presence of 0.2M NaCl activity decreased 40–75%	Uchimura K, Miyazaki M, Nogi Y, Kobayashi T, Horikoshi K. (2010). Cloning and sequencing of alginate lyase genes from deep-sea strains of *Vibrio* and *Agarivorans* and characterization of a new *Vibrio* enzyme. Mar Biotechnol (NY) 12:526-533.
Deep-sea clam *Calyptogena kaikoi*, which inhabits depths exceeding 3,500 m	1 Arginine kinase	Opt. pH: 7.9 Opt Temp.: 10ºC Salt dependence: not reported	Suzuki T, Yamamoto K, Tada H, Uda K. (2012). Cold-adapted features of arginine kinase from the deep-sea clam *Calyptogena kaikoi*. Mar Biotechnol (NY) 14:294-303.
Nocardiopsis sp. 7326 from deep sea sediment of Prydz Bay, Antarctic	1 α-Amylase	Opt. pH: 8.0 Opt Temp.: 35ºC Salt dependence: not affected by NaCl and KCl	Zhang JW, Zeng RY. (2008). Purification and characterization of a cold-adapted alpha-amylase produced by *Nocardiopsis* sp. 7326 isolated from Prydz Bay, Antarctic. Mar Biotechnol (NY) 10:75-82.
Deep-sea piezophilic bacterium, *Shewanella violacea* strain DSS12	1 RNA polymerase	Opt. pH: not reported Opt Temp.: not reported Salt dependence: not reported	Kawano H, Nakasone K, Abe F, Kato C, Yoshida Y, Usami R, Horikoshi K. (2005). Identification of rpoBC genes encoding for beta and beta' subunits of RNA polymerase in a deep-sea piezophilic bacterium, *Shewanella violacea* strain DSS12. Biosci Biotechnol Biochem 69:575-582
Deep-sea yeast, *Cryptococcus liquefancis* strain N6	1 Polygalacturonase	Opt. pH: not reported Opt Temp.: 10ºC Salt dependence: not reported	Abe F, Minegishi H, Miura T, Nagahama T, Usami R, Horikoshi K. (2006). Characterization of cold- and high-pressure-active polygalacturonases from a deep-sea yeast, *Cryptococcus liquefaciens* strain N6. Biosci Biotechnol Biochem 70:296-299.
Deep-sea heavy-metal-tolerant yeast *Cryptococcus liquefaciens* strain N6	1 Copper/zinc superoxide dismutase	Opt. pH: not reported Opt Temp.: not reported Salt dependence: not reported	Kanamasa S, Sumi K, Yamuki N, Kumasaka T, Miura T, Abe F, Kajiwara S. (2007). Cloning and functional characterization of the copper/zinc superoxide dismutase gene from the heavy-metal-tolerant yeast *Cryptococcus liquefaciens* strain N6. Mol Genet Genomics 277:403-412.

Deep-sea bacterium *Oceanobacillus iheyensis*, from the sediment at a depth of 1050 meters in the Pacific Ocean	1 Antibiotic resistant enzyme	Opt. pH: not reported Opt Temp.: not reported Salt dependence: not reported	Toth M, Smith C, Frase H, Mobashery S, Vakulenko S. (2010). An antibiotic-resistance enzyme from a deep-sea bacterium. J Am Chem Soc 132:816-823.
Piezophilic bacterium *Photobacterium profundum* strain SS9	1 Cytochrome P450	Opt. pH: not reported Opt Temp.: not reported Salt dependence: not reported	Sineva EV, Davydov DR. (2010). Cytochrome P450 from *Photobacterium profundum* SS9, a piezophilic bacterium, exhibits a tightened control of water access to the active site. Biochemistry 49:10636-10646.
Deep-sea extremely halotolerant and alkaliphilic *Oceanobacillus iheyensis* HTE831	1 Nicotinamidase	Opt. pH: 6.0-6.5 Opt Temp.: 45ºC Salt dependence: not reported	Sánchez-Carrón G, García-García MI, Zapata-Pérez R, Takami H, García-Carmona F, Sánchez-Ferrer A. (2013). Biochemical and mutational analysis of a novel nicotinamidase from *Oceanobacillus iheyensis* HTE831. PLoS One 8:e56727.
Halorubrum lacusprofundi, an extremely halophilic microbe from deep lake in Antarctica	1 β-Galactosidase	Opt. pH: not reported Opt Temp.: not reported Salt dependence: not reported	Dassarma S, Capes MD, Karan R, Dassarma P. (2013). Amino acid substitutions in cold-adapted proteins from *Halorubrum lacusprofundi*, an extremely halophilic microbe from antarctica. PLoS One 8:e58587.
Deep-sea shrimp, *Oplophorus gracilirostris*	1 Luciferase	Opt. pH: not reported Opt Temp.: 4-15ºC Salt dependence: not reported	Inouye S, Sasaki S. (2007). Overexpression, purification and characterization of the catalytic component of *Oplophorus* luciferase in the deep-sea shrimp, *Oplophorus gracilirostris*. Protein Expr Purif 56:261-268.
Riftia pachyptila, a symbiotic invertebrate from deep-sea hydrothermal vents at 2600-m depth along the East Pacific Rise	Carbonic Anhydrases	Opt. pH: not reported Opt Temp.: not reported Salt dependence: not reported	De Cian MC, Bailly X, Morales J, Strub JM, Van Dorsselaer A, Lallier FH. (2003). Characterization of carbonic anhydrases from *Riftia pachyptila*, a symbiotic invertebrate from deep-sea hydrothermal vents. Proteins 51:327-339.
Microbulbifer sp. strain JAM-3301, from deep-sea sediments collected from Sagami Bay, Japan (35°04.989′N, 139°13.015′E) at a water depth of 900 m	Inulinase and Fructofuranosidase	Opt. pH: 8.0-9.0 Opt Temp.: 35ºC Salt dependence: not reported	Kobayashi T, Uchimura K, Deguchi S, Horikoshi K. (2012). Cloning and sequencing of inulinase and β-fructofuranosidase genes of a deep-sea *Microbulbifer* species and properties of recombinant enzymes. Appl Environ Microbiol 78:2493-2495.
Deep-sea uncultivable microbes			
Deep-sea sediment metagenome taken from a clam bed community from Edison Seamount, south of Lihir Island in the New Ireland Fore-arc near Papua New Guinea	1 Esterase	Opt. pH: 10.0 Opt Temp.: 50-55ºC Salt dependence: not reported	Park HJ, Jeon JH, Kang SG, Lee JH, Lee SA, Kim HK. (2007). Functional expression and refolding of new alkaline esterase, EM2L8 from deep-sea sediment metagenome. Protein Expr Purif 52:340-347.
Deep-sea sediment at Edison Seamount (3°89′Σ, 152°49′E; depth 1,440 m)	1 Lipase	Opt. pH: 8.0 Opt Temp.: 30ºC (retaining about 60% activity at 5ºC) Salt dependence: only tested at 1 mM	Jeon JH, Kim JT, Kim YJ, Kim HK, Lee HS, Kang SG, Kim SJ, Lee JH. (2009). Cloning and characterization of a new cold-active lipase from a deep-sea sediment metagenome. Appl Microbiol Biotechnol 81:865-874.
Deep-sea marine sediment sample from South China Sea	1 Esterase	Opt. pH: 7.0-10.0 Opt Temp.: 50ºC Salt dependence: not reported	Fu C, Hu Y, Xie F, Guo H, Ashforth EJ, Polyak SW, et al. (2011). Molecular cloning and characterization of a new cold-active esterase from a deep-sea metagenomic library. Appl Microbiol Biotechnol 90:961-970.

Deep-sea sediments from the skirt of a seamount in the middle of the Pacific Ocean at a water depth of 5,886 m	9 Esterases	Opt. pH: 7.5 Opt Temp.: 20°C Salt dependence: not reported	Jiang X, Xu X, Huo Y, Wu Y, Zhu X, Zhang X, Wu M. (2012). Identification and characterization of novel esterases from a deep-sea sediment metagenome. Arch Microbiol 194:207-214.
Pacific deep-sea sediment at the East Pacific nodule province. The depth of this site is 5,274 m, temperature 1.5_C and the salinity 35‰.	2 Alkane hydroxylases	Opt. pH: - Opt Temp.: - Salt dependence: - not reported	Xu M, Xiao X, Wang F. (2008). Isolation and characterization of alkane hydroxylases from a metagenomic library of Pacific deep-sea sediment. Extremophiles 12:255-262.
Piezophilic bacteria from intestinal contents of deep-sea fishes retrieved from the abyssal zone	11 Malate dehydrogenases	Opt. pH: not reported Opt Temp.: not reported Salt dependence: not reported	Saito R, Kato C, Nakayama A. (2006). Amino acid substitutions in malate dehydrogenases of piezophilic bacteria isolated from intestinal contents of deep-sea fishes retrieved from the abyssal zone. J Gen Appl Microbiol 52:9-19.
Deep anoxic hypersaline lakes in the eastern Mediterranean sea	Catechol 2,3-dioxygenase genes	Opt. pH: not reported Opt Temp.: not reported Salt dependence: not reported	Brusa T, Borin S, Ferrari F, Sorlini C, Corselli C, Daffonchio D. (2011). Aromatic hydrocarbon degradation patterns and catechol 2,3-dioxygenase genes in microbial cultures from deep anoxic hypersaline lakes in the eastern Mediterranean sea. Microbiol Res 156:49-58.
Mmarine sediments in southwest Japan	Chitinases	Opt. pH: not reported Opt Temp.: not reported Salt dependence: not reported	Bhuiyan, F.A., Nagata, S., and Ohnishi, K. (2011). Novel chitinase genes from metagenomic DNA prepared from marine sediments in southwest Japan. Pak J Biol Sci 14:204–211.
Neritic sediments of the South China Sea	1 Esterase	Opt. pH: 8.6 Opt Temp.: 40°C Salt dependence: not reported	Peng Q, Zhang X, Shang M, Wang X, Wang G, Li B, *et al.* (2011). A novel esterase gene cloned from a metagenomic library from neritic sediments of the South China Sea. Microb Cell Fact 10:95.
Deep-sea sediment from Qiongdongnan Basin, South China Sea		Opt. pH: not reported Opt Temp.: not reported Salt dependence: not reported	Hu Y, Fu C, Yin Y, Cheng G, Lei F, Yang X, *et al.* (2010). Construction and preliminary analysis of a deep-sea sediment metagenomic fosmid library from Qiongdongnan Basin, South China Sea. Mar Biotechnol (NY) 12:719-727.
Juan de Fuca Ridge hydrothemal vent	1 GH57 glycosidase	Opt. pH: 7.5 Opt Temp.: 90°C Salt dependence: tested with NaCl at 50 mM (no effect)	Wang H, Gong Y, Xie W, Xiao W, Wang J, Zheng Y, *et al.* (2011). Identification and characterization of a novel thermostable gh-57 gene from metagenomic fosmid library of the Juan de Fuca Ridge hydrothemal vent. Appl Biochem Biotechnol 164:1323-1338.
Urania deep-sea hypersaline anoxic basin	5 Esterases	Opt. pH: 10.0-12.0 Opt Temp.: 40-60°C Salt dependence: Na^+ and/or K^+ ions strongly stimulated the activity of three enzymes and mildly stimulated one	Ferrer M, Golyshina OV, Chernikova TN, Khachane AN, Martins Dos Santos VA, Yakimov MM, *et al.* (2005). Microbial enzymes mined from the Urania deep-sea hypersaline anoxic basin. Chem Biol 12:895-904.
Deep-sea (un)cultivable microbes with structures available			
Extreme psychrophilic bacterium *Moritella profunda*	1 Aspartate carbamoyltransferase	Opt. pH: 9.0-10.0 Opt Temp.: 0-15°C Salt dependence: not reported	De Vos D, Xu Y, Hulpiau P, Vergauwen B, Van Beeumen JJ. (2007). Structural investigation of cold activity and regulation of aspartate carbamoyltransferase from the extreme psychrophilic bacterium *Moritella profunda*. J Mol Biol 365:379-395.
Halotolerant and alkaliphilic, strictly aerobic, Gram-positive bacterium *Oceanusbacillus iheyensis*, from Iheya Ridge at a depth of 1050 m	1 β-Lactamase	Opt. pH: not reported Opt Temp.: not reported Salt dependence: not reported	Pietra F. (2012). On 3LEZ, a deep-sea halophilic protein with in vitro class-a β-lactamase activity: molecular-dynamics, docking, and reactivity simulations. Chem Biodivers 9:2659-2684.
Eukaryotic thermophile	1 Superoxide dismutase	Opt. pH: not reported	Shin DS, Didonato M, Barondeau DP, Hura GL, Hitomi C, Berglund JA, *et al.* (2009). Superoxide dismutase

Alvinella pompejana, a deep-sea hydrothermal-vent worm that has been found in temperatures averaging as high as 68 °C, with spikes up to 84 °C		Opt Temp.: not reported Salt dependence: not reported	from the eukaryotic thermophile *Alvinella pompejana*: structures, stability, mechanism, and insights into amyotrophic lateral sclerosis. J Mol Biol 385:1534–1555.
Geobacillus sp. strain HTA-462, the deepest sea bacteria, found in the sediment sample collected from the bottom of the Challenger Deep in the Mariana Trench at a depth of 10,897 m	1 GH13 α-glucosidase	Opt. pH: 9.0 Opt Temp.: 60°C Salt dependence: 1.6-activated by 10 mM $MgCl_2$	Shirai T, Hung VS, Morinaka K, Kobayashi T, Ito S. (2008). Crystal structure of GH13 alpha-glucosidase GSJ from one of the deepest sea bacteria. Proteins 73:126-133.
Deep-sea bacterium *Oceanobacillus iheyensis*, from the sediment at a depth of 1050 meters in the Pacific Ocean	1 Antibiotic resistant enzyme	Opt. pH: not reported Opt Temp.: not reported Salt dependence: not reported	Toth M, Smith C, Frase H, Mobashery S, Vakulenko S. (2010). An antibiotic-resistance enzyme from a deep-sea bacterium. J Am Chem Soc 132:816-823.

Table S2 Hydrochemistry of selected deep-sea regions, deep-sea libraries and esterase screening statistics.

Variable	*Medee*	*Kryos*	*Bannock*	*Matapan*
Density (g/L)	1.22	1.30	1.12	1.027
Depth (m)	3,010	3,340	3,342	4,908
Na^+ (g/Kg)	106.96	3.70	79.04	10.56
K^+	18.07	1.13	4.03	0.46
Ca^{2+}	1.21	0.03	0.56	0.42
Mg^{2+}	18.07	94.77	12.32	1.41
Cl^-	171.45	184.00	156.26	21.20
SO_4^{2-}	32.04	30.29	10.82	2.95
Salinity (g/Kg)	347.80	313.92	263.20	38.6
Temp. (ºC)	14.75-15.46	16.5	14.5	14.29
pH	6.87	6.7	6.55	8.12
Clones screen	15,744	5,280	15,000	4,000
Clones select	2	1	1	1

Table S3. General features and residues potentially involved in catalysis, substrate recognition and thermal and halophilic adaptations in the proteins investigated. Panel A, General features of esterase-like proteins. Panel B, Percentage of identity between esterases with the α/β hydrolase fold as determined by the Matcher (EMBOSS package). Matches/alignment lengths (% identity) are specifically indicated. Panel C, General features of proteins characterised from the *Medee* basin other than esterases. Panel D, thermophilic adaptations for proteins with determined crystal structures. Panel E, halophilic adaptations for proteins with determined crystal structures. Panel F, High-pressure adaptations for proteins with determined crystal structures.

(A) General features of esterase-like proteins

	MGS-B1	**MGS-K1**	**MGS-M1**	**MGS-M2**	**MGS-MT1**	**MGS-HA1**
MW (Da)	34,551.8	56,234.1	26,801.8	31,602.2	35,651.6	28,862.7
*p*I	4.38	4.89	5.77	5.39	7.29	5.99
Amino acid	316	514	239	276	323	261
Catalytic triad	S160 D255 H285	S196E321 H424	S113 D169 H201	S97 D221 H249	S194 D290 H320	S115 D153 H235
GXSXG-lipase motif[a]	G158-D159-S160-A161-G162-G163	G194-E195-S196-A197-G198-A199	G111-F112-S113-A114-G115-G116	G95-I96-S97-Y98-G99-A100	G192-T193-S194-A195-G196-G197	G113-H114-S115-L116-G117-G118
Oxyanion hole motif[a]	H86-G87-G88-G89-F90	H108-G109-G110-A111-F112	P40-G41-G42-G43-Y44	N30-G31-I32-M33-M34	H125-G126-G127-A128-Y129	H37-G38-F39-I40-G41
Classified family	IV	III	Unclassified (possibly IV)	V	IV	V
Closest sequence homolog in NCBI (% identity via BLAST)	AEM45131.1 (51%)	YP_004858757.1 (44%)	YP_004858591.1 (49%)	YP_001620501.1 (48%)	YP_004469213.1 (62%)	YP_004984003.1 (99%)
Closest sequence homolog in PDB (% identity via BLAST)	2YH2 (48%)	2OGT (39%)	3BXP (30%)	3OM8 (25%)	3V9A (28%)	3PF8 (26%)
Closest structural homolog in PDB (% identity, RMSD via PDBeFold)	N/A	N/A	4BZW (31%, 1.2 Å over 190 Cα)	2XUA (23%, 1.8 Å over 253 Cα)	3G9Z (24%, 1.6 Å over 283 Cα)	N/A

[a]Consensus GXSXG-lipase motifs for families, according to Kourist *et al.* (2010):
family II = GHSXGG
family III = GESAGA
family IV = GDSAGG
family V = GNSMGG

[b]Consensus oxyanion hole motifs for families, according to Kourist *et al.* (2010):
family II = HGX-X
family III = HGGGF
family IV = HGGGF
family V = HGSG-
family VI = NGGPG

(B) Percentage of identity between esterases with the α/β hydrolase fold as determined by the Matcher (EMBOSS package). Matches/alignment lengths (% identity) are specifically indicated.

	MGS-B1	**MGS-HA1**	**MGS-K1**	**MGS-M1**	**MGS-M2**	**MGS-MT1**
MGS-B1		56/381 (14.7%)	95/542 (17.5%)	65/351 (18.5%)	58/374 (15.5%)	80/367 (21.8%)
MGS-HA1	56/381 (14.7%)		31/675 (4.6%)	52/311 (16.7%)	55/319 (17.2%)	25/494 (5.1%)
MGS-K1	95/542 (17.5%)	31/675 (4.6%)		50/600 (8.3%)	62/554 (11.2%)	76/559 (13.6%)
MGS-M1	65/351 (18.5%)	52/311 (16.7%)	50/600 (8.3%)		42/327 (12.8%)	60/359 (16.7%)
MGS-M2	58/374 (15.5%)	55/319 (17.2%)	62/554 (11.2%)	42/327 (12.8%)		56/393 (14.2%)
MGS-MT1	80/367 (21.8%)	25/494 (5.1%)	76/559 (13.6%)	60/359 (16.7%)	57/394 (14.5%)	

(C) General features of proteins characterised from the *Medee* basin other than esterases

	MGS-M3	**MGS-M4**	**MGS-M5**
MW (Da)	84,278.59	31,792.29	34,792.79
pI	5.55	5.95	6.21
Amino acid	734	274	314
Closest sequence homolog in NCBI (% identity via BLAST)	WP_006447913.1 (41%)	YP_003966442.1 (54%)	YP_001621014.1 (72%)
Closest sequence homolog in PDB (% identity via BLAST)	2X40_A (34%)	4FZI_A (52%)	1LDB_A (52%)
Catalytic site	D225* E408*	Y48 H106 K73 D43	H176 D149 R152 A220 T230 N121

* Experimentally confirmed by site-directed mutagenesis.

(D) Thermophilic adaptations for proteins with determined crystal structures

		MGS-M2 vs. 2WUG	**MGS-MT1 vs. 3DNM**	**MGS-M1 vs. 4BZW**	**MGS-M5 vs. 3PQD**	**MGS-M4 vs. 1RY0**
Optimal temperature range		60-70 deg. C	40-50 deg. C	25-30 deg. C	only tested at 30 deg. C	4-22 deg. C
Interactions	More H-bonds	-	+	-	+	-
	More salt bridges	-	-	+	+	-
	More aromatic-aromatic interactions	+	-	+	+	+
	More disulfides	equal	equal	equal	equal	equal
Charged amino acid content	Decreased surface negative charge	+	-	+	+	+
	More total charged residues	-	-	+	+	-
	Lower Glu+Asp / Lys+Arg ratio	-	+	-	+	+
	Higher Arg/Lys ratio	-	+	-	+	-
Other amino acid content	Less Gly	+	+	+	+	+
	Less His	+	+	+	-	-
	More Ile	+	+	equal	+	+
	Less Met	equal	-	equal	-	-
	More Pro (loops)	-	+	+	+	-
	Less Pro (helices)	-	+	+	+	+
Hydrophobicity	Increase in core	-	-	+	+	+
	Decrease in surface	+	+	+	+	+

(E) Halophilic adaptations for proteins with determined crystal structures

		MGS-M2 vs. 2WUG	**MGS-M1 vs. 4BZW**	**MGS-MT1 vs. 3DNM**	**MGS-M4 vs. 1RY0**	**MGS-M5 vs. 3PQD**
Salt tolerance		hyperactivation at 3 M	hyperactivation at 3 M	hyperactivation at 3 M	constant activity up to 1 M	40% loss of activity at 1 M
Charged amino acid content	Decrease in overall pI	+	+	-	+	-
	Increase in surface Glu/Asp	even	+	-	-	+
	Less Lys	-	-	+	+	-
Hydrophobicity	Decrease in buried apolar surface	+	+	-	+	-
	Less Leu/Ile	-	+	+	-	-
	Less Phe/Trp/Tyr	-	+	-	-	+
	More Gly/Ala/Val	-	-	+	-	-

(F) High-pressure adaptations for proteins with determined crystal structures

		MGS-M2 vs. 2WUG	**MGS-M1 vs. 4BZW**	**MGS-MT1 vs. 3DNM**	**MGS-M4 vs. 1RY0**	**MGS-M5 vs. 3PQD**
Pressure tolerance		Pressure tolerant	Inactivated by pressure	Activated by pressure	Inactivated by pressure	Inactivated by pressure
Hydrophobic core	Smaller size	+	-	-	+	-
	Increased ratio small/large amino acids	-	+	+	-	-
Interactions	Less salt bridges	+	-	+	-	+
Oligomerization	More oligomerization	-	-	-	+	-
Hydrophobic core	Smaller size	+	-	-	+	-
	Increased ratio small/large amino acids	-	+	+	-	-

Table S4 Compositional similarities between the DNA fragments containing the genes of interest and bacterial genomes as shown by GOHTAM and TBLASTX analyses.

Enzyme ID	GOHTAM	Local TBLASTX against NCBI nt database (sharing of protein coding genes)		
		5 best hits	Scores	Taxonomic level of identification by MEGAN5
MGS-M1	*Eubacterium biforme* (genome) 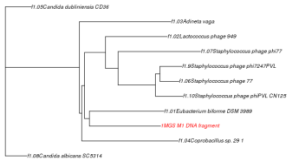	*Clostridium novyi* NT	734.0	Bacteria
		Desulfitobacterium hafniense DCB-2	721.0	
		Desulfitobacterium hafniense Y51	720.0	
		Clostridium acetobutylicum ATCC 824	719.0	
		Clostridium tetani E88	717.0	
MGS-M2 MGS-M3 MGS-M4 MGS-M5	*Eubacterium biforme* (genome) 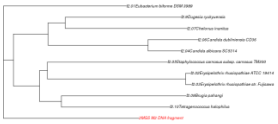	*Acholeplasma laidlawii* PG-8A	643.0	Bacteria
		Fusobacterium nucleatum subsp. nucleatum ATCC 25586	632.0	
		Thermoanaerobacter tengcongensis MB4	624.0	
		Thermoanaerobacter sp. X514	617.0	
		Thermoanaerobacter pseudethanolicus ATCC 33223	610.0	
MGS-HA1	*Geobacillus* sp. (genome) 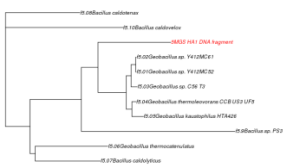	*Geobacillus kaustophilus* HTA426	3265.0	*Geobacillus kaustophilus*
MGS-MT1	*Alteromonas macleodii* (genome) 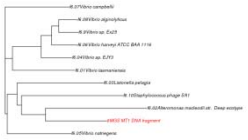	*Pseudoalteromonas atlantica* T6c	2851.0	Alteromonadales
		Idiomarina loihiensis L2TR	2631.0	
		Shewanella amazonensis SB2B	2620.0	
		Colwellia psychrerythraea 34H	2570.0	
MGS-B1	Plasmid like contig 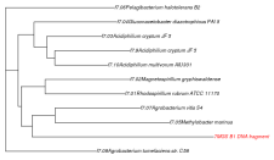	*Variovorax paradoxus* S110	322.0	*Variovorax paradoxus*
MGS-K1	*Aspergillus* sp. 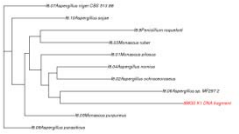	*Candidatus Accumulibacter phosphatis*	341.0	Not identified
		Desulfitobacterium hafniensis Y51	317.0	

Table S5 List of primers used in the study.

Name	Sequence
ESTERASES	
MGS-M1Fwd	*5′*-GACGACGACAAGATGAATATAAGTAAGATAAC-*3′*
MGS-M1Rev	*5′*-GAGGAGAAGCCCGGTTATAAATCAAGTAC-*3′*
MGS-M2Fwd	*5′*-GACGACGACAAGGTGAGTATATTTACATATCAAG-*3′*
MGS-M2Rev	*5′*-GAGGAGAAGCCCGGCTAAATTTGATAATCTAGTTTC-*3′*
MGS-MT1wd	*5′*-GACGACGACAAGATCGGGGAACAGGCTAAAGAGG-*3′*
MGS-MT1Rev	*5′*-GAGGAGAAGCCCGGTTAATTCGTAAAGCCCACCAAAAAAC-*3′*
MGS-B1Fwd	*5′*-GACGACGACAAGATGACGCTGGATGCGCAGG-*3′*
MGS-B1Rev	*5′*-GAGGAGAAGCCCGGTTACTAGTTTGTTTCGGCGAAGGC-*3′*
MGS-K1Fwd	*5′*-TTGTATTTCCAGGGCATGAGCAATAATAAACAAACCGTAG-*3′*
MGS-K1Rev	*5′*-CAAGCTTCGTCATCAGGGCATAGCCGATTTATAGG-*3′*
MGS-HA1Fwd	*5′*-GACGACGACAAGATGTTGATTCGATTCCAGTATATTG-*3′*
MGS-HA1Rev	*5′*-AGGAGAAGCCCGGTTACTAGACGACCACCGCACGTTGG-*3′*
OTHER ENZYMES	
MGS-M3Fwd	*5′*-GACGACGACAAGATGAAAAAAATACCTCTAGAAG-*3′*
MGS-M3Rev	*5′*-GAGGAGAAGCCCGGTTATACATTGATATCCTC-*3′*
MGS-M4Fwd	*5′*-TTGTATTTCCAGGGCATGCATAGTGTAAAACTAAACAAC-*3′*
MGS-M4Rev	*5′*-CAAGCTTCGTCATCAGTAATCTACGTTATCAAATTCAG-*3′*
MGS-M5Rev	*5′*-TTGTATTTCCAGGGCATGAGAAATAGCAAAGTGGTAG-*3′*
MGS-M5Fwd	*5′*- AAGCTTCGTCATCAATAGCTCATATCATCTAGGTTTTTACGT*3′*

Table S6 X-ray diffraction statistics.

Enzyme	**MGS-M1**	**MGS-M2**	**MGS-M4**	**MGS-M5**	**MGS-MT1**
PDB code	4Q3K	4Q3L	4Q3M	4Q3N	4Q3O
Data collection					
Space group	C2	$P2_1$	$P6_4$	$P4_122$	C2
Cell dimensions					
a, *b*, *c* (Å)	78.99, 82.71, 77.38	105.57, 139.13, 111.11	172.47, 172.47, 113.06	92.82, 92.82, 203.80	189.45, 131.40, 112.44
α, β, γ (°)	90, 109.32, 90	90, 89.94, 90	90, 90, 120	90, 90, 90	90, 103.55, 90
Resolution (Å)	30.00 – 1.57	32.00 – 3.00	25.00 – 2.55	35.00 – 1.97	19.72 – 1.74
Number of unique reflections	63876	63183	59489	31973	272067
R_{merge}	0.042 (0.485)[a]	0.093 (0.536)[b]	0.119 (0.718)[c]	0.048 (0.510)[d]	0.056 (0.392)[e]
$I / \sigma I$	30.19 (2.09)	17.08 (3.66)	19.05 (3.01)	45.3 (5.31)	21.3 (2.2)
Completeness (%)	97.8 (83.0)	99.9 (100)	95.8 (99.9)	99.9 (99.9)	99.6 (100)
Redundancy	2.8 (2.4)	4.6 (4.6)	4.4 (4.3)	6.1 (6.0)	3.0 (2.9)
Refinement					
Resolution (Å)	28.30 – 1.57	31.67 – 3.01	24.58 – 2.55	34.31 – 1.97	19.72 – 1.74
No. of reflections: working, test	63864, 3341	63067, 1992	59408, 1989	31945, 1998	271732, 13720
R-factor$_{work}$, *R*-factor$_{free}$	14.6, 18.6	20.0, 25.5	20.7, 26.6	14.5, 18.4	14.4, 18.5
Average *B*-factors					
Protein	25.9	58.8	56.5	33.9	20.8
Solvent	52.8	76.8	56.3	50.0	39.9
Water	42.8	41.3	49.6	70.3	38.5
R.m.s. deviations					
Bond lengths (Å)	0.009	0.004	0.005	0.017	0.015
Bond angles (°)	1.221	0.711	0.757	1.489	1.483
Ramachandran analysis					
Most favoured (%)	89.1	89.2	89.6	89.6	90.1
Additionally allowed	9.5	10.3	9.6	9.6	8.7
Generously allowed	1.0	0.1	0.8	0.8	0.5
Disallowed	0.5*	0.4*	0	0	0.7*

Values in parentheses refer to highest resolution shell: [a]1.60-1.57 Å, [b]3.05-3.00, [c]2.59-2.55, [d]2.00-1.97, [e]1.83-1.74

*Residues in disallowed regions correspond to MGS-M1 Ser113 (catalytic), MGS-M2 Ser97 (catalytic), MGS-MT1 Ile245.

Fig. S1 pH profiles of wild-type enzymes. The specific activities were calculated in triplicate as described in the Experimental procedures. The standard deviation (SD) is shown. The 100% activity is as shown in Table 1. Note: due to protein instability at low pH, the pH profile for MGS-M5 could not be obtained; preliminary test reactions indicated pH 8.0 (50 mM Tris-HCl) as being the most suitable buffer for activity determinations, and this value was used as the standard buffer for this enzyme.

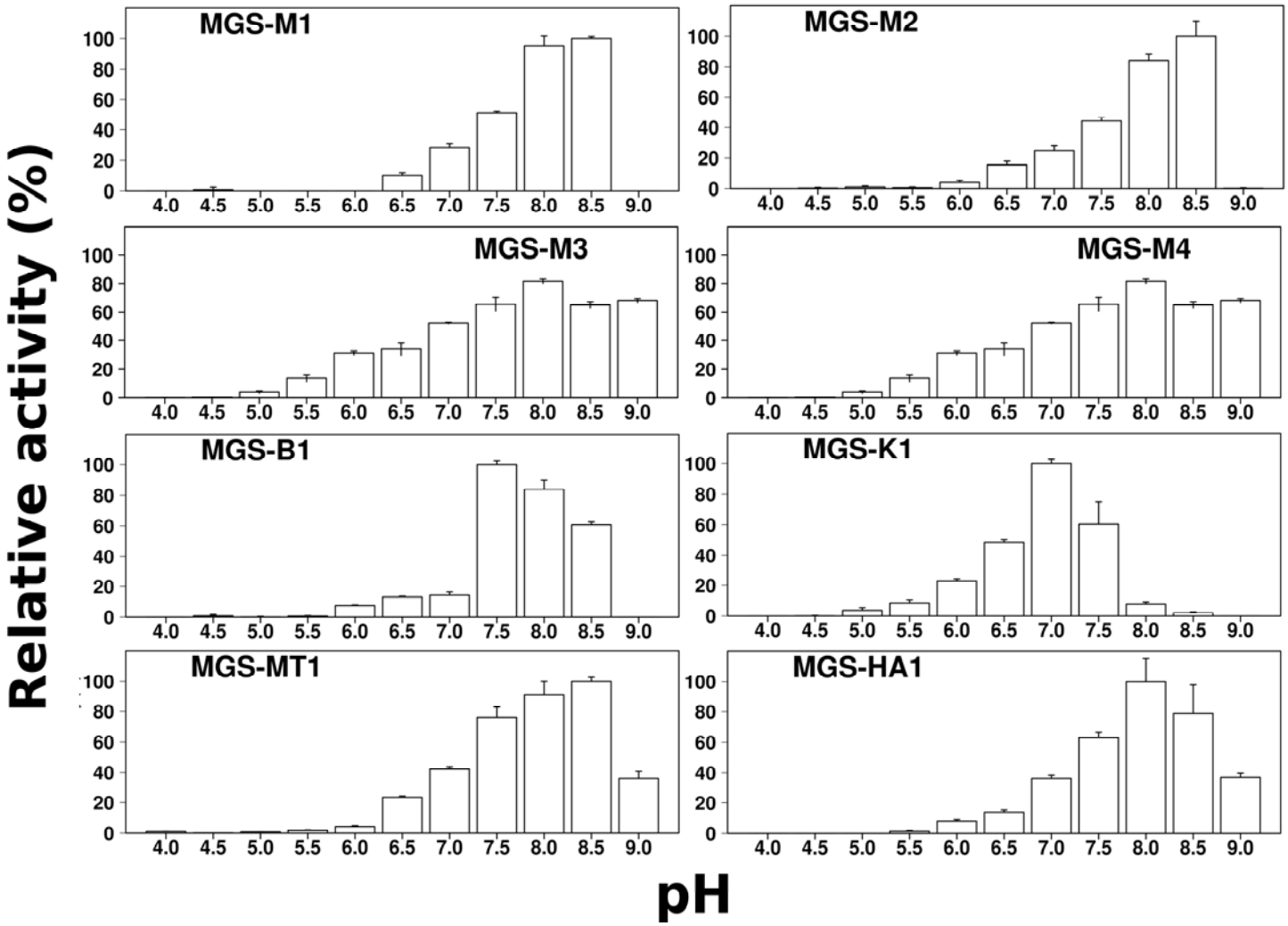

Fig. S2 Substrate profiles of the enzymes with a set of structurally diverse substrates. The specific activities were calculated in triplicate as described in the Experimental procedures, using the standard assay conditions (see also summary conditions in Table 1). Mean values (in log scale) are given. The standard deviation (SD) is not shown due to the logarithmic scale, but it is ≤ 0.23%. Note: using standard conditions for MGS-M3, no activity was detected using *p*NP-α-glucose, *p*NP-α-maltooligosaccharides (C2 to C6), *p*NP-α-galactose, *p*NP-β-galactose, *p*NP-α-xylose, *p*NP-β-arabinopyranose, *p*NP-α-rhamnose, *p*NP-α-mannose, *p*NP-β-mannose, *p*NP-α-fucose, *p*NP-β-glucuronide, carboxymethyl cellulose, laminarin, lichenan and crystalline cellulose.

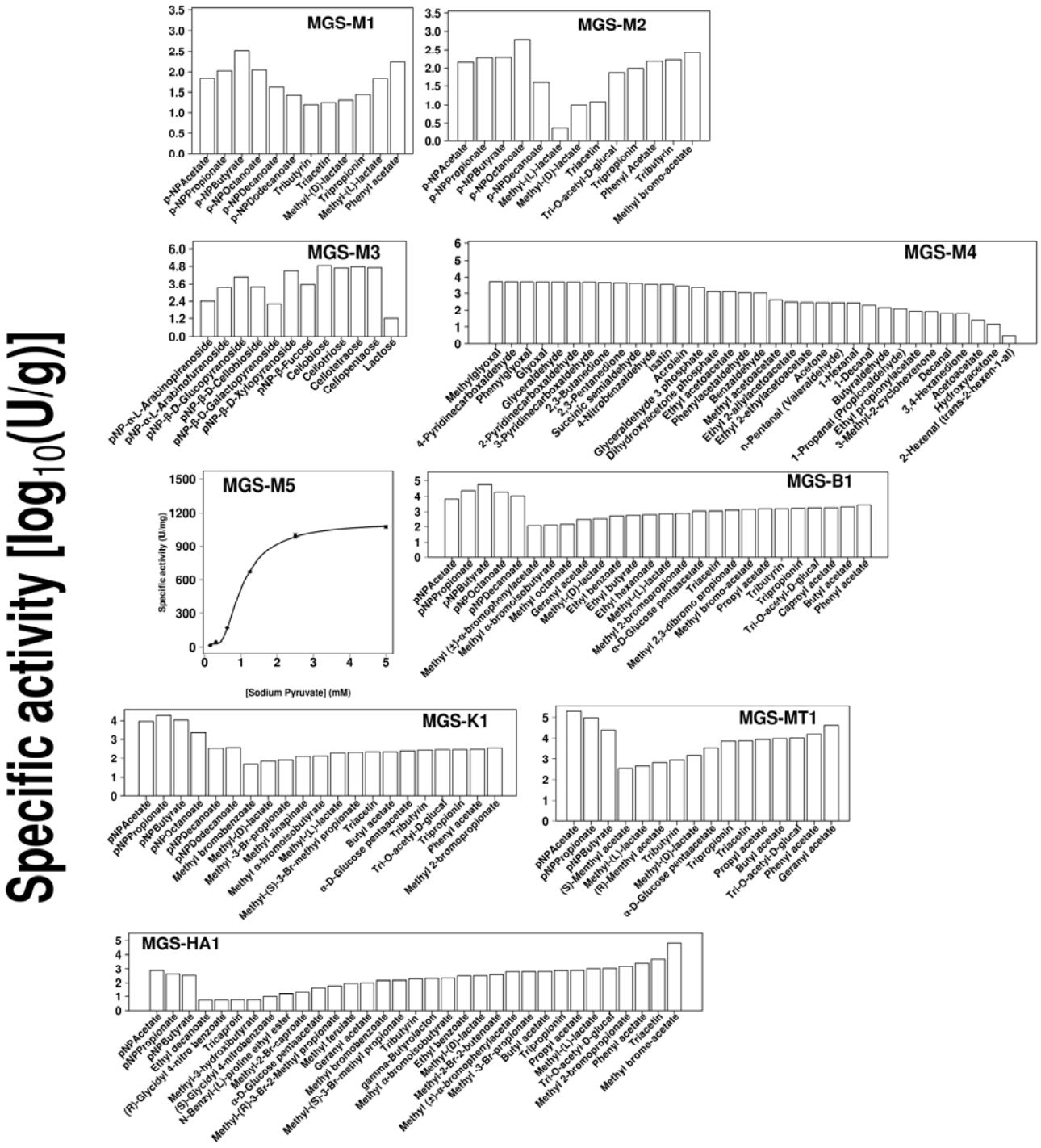

Fig. S3 Comparison of the structures of MGS enzymes crystallised in this study and their structural homologues revealed by structure similarity searches. Enzymes are shown as cartoon representations. Arrows refer to the locations of the catalytic serine (for esterases in top row) or the NADPH/NADH and substrate binding sites (for bottom row enzymes).

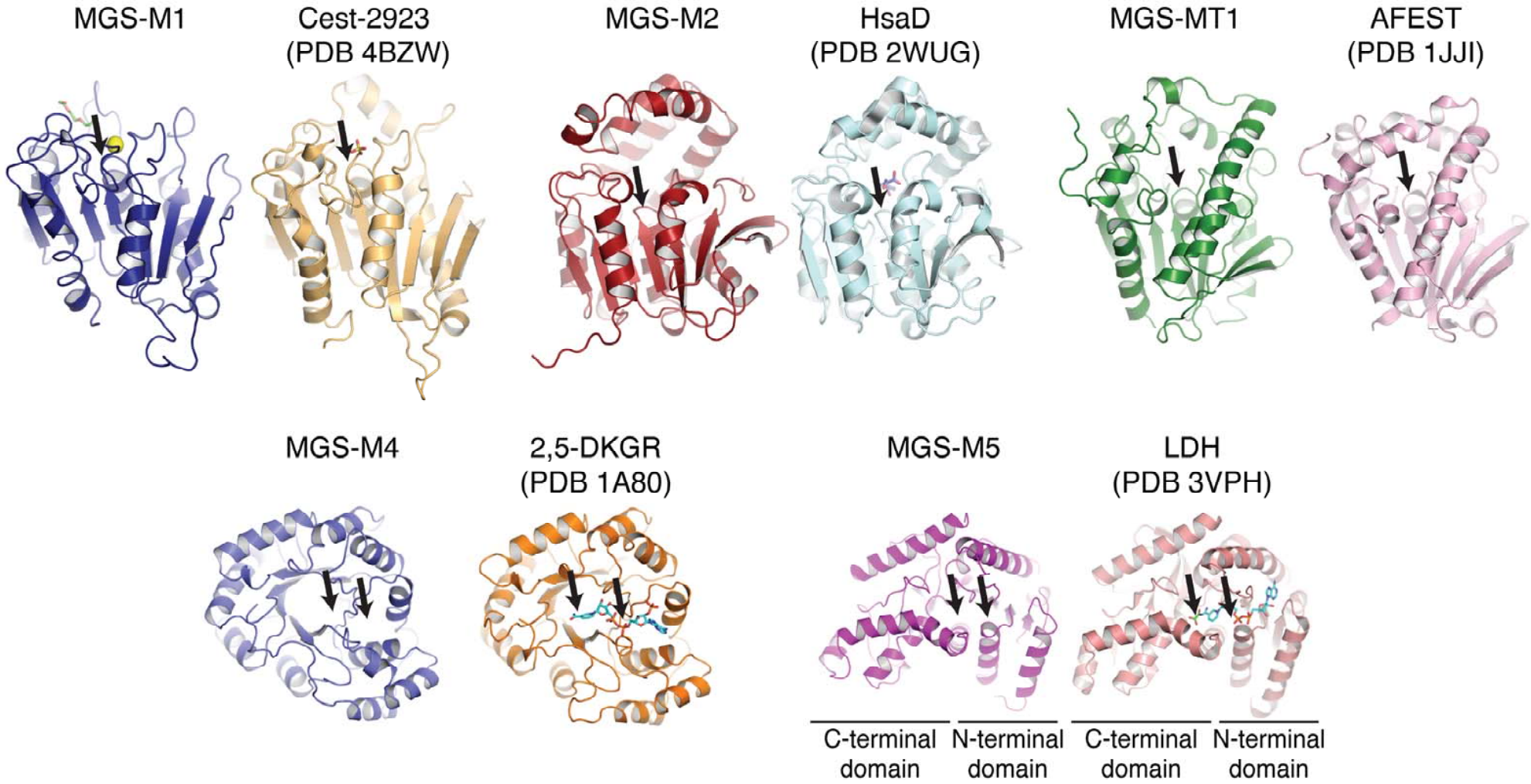

Fig. S4 Comparison of putative active sites of MGS enzymes crystallised in this study and their structural homologues revealed by structure similarity searches. Sticks are shown for bound substrates and residues predicted to participate in catalytic reactions and/or interact with substrates. The catalytic triads for the esterases in the top row are labelled. The substrate-binding canals for MGS-M2 and HsaD are also shown in solvent-accessible surface representations, coloured by electrostatic potential, highlighting the disparate charge features, which are shown under their respective cartoon images. The non-NADH/NADPH substrate-binding residues for 2,5-DKGR and LDH, plus the equivalent residues in MGS-M4 and MGS-5, are labelled.